The tetramer structure of the Nervy homology two domain, NHR2, is critical for AML1/ETO's activity

Yizhou Liu,[1,7] Matthew D. Cheney,[2,7] Justin J. Gaudet,[2] Maksymilian Chruszcz,[1] Stephen M. Lukasik,[3] Daisuke Sugiyama,[2] Jeff Lary,[4] James Cole,[4,5] Zbyszek Dauter,[6] Wladek Minor,[1] Nancy A. Speck,[2,*] and John H. Bushweller[1,3,*]

[1] Department of Molecular Physiology and Biological Physics, University of Virginia, Charlottesville, Virginia 22908
[2] Department of Biochemistry, Dartmouth Medical School, Hanover, New Hampshire 03755
[3] Department of Chemistry, University of Virginia, Charlottesville, Virginia 22906
[4] National Analytical Ultracentrifugation Facility, University of Connecticut, Storrs, Connecticut 06269
[5] Department of Molecular and Cell Biology, University of Connecticut, Storrs, Connecticut 06269
[6] Macromolecular Crystallography Laboratory, National Cancer Institute, Brookhaven National Laboratory, Upton, New York 11973
[7] These authors contributed equally to this work.
*Correspondence: nancy.speck@dartmouth.edu (N.A.S.); jhb4v@virginia.edu (J.H.B.)

Summary

AML1/ETO is the chimeric protein resulting from the t(8;21) in acute myeloid leukemia. The Nervy homology 2 (NHR2) domain in ETO mediates oligomerization and AML1/ETO's interactions with ETO, MTGR1, and MTG16, and with the corepressor molecules mSin3A and HDAC1 and HDAC3. We solved the NHR2 domain structure and found it to be an α-helical tetramer. We show that oligomerization contributes to AML1/ETO's inhibition of granulocyte differentiation, is essential for its ability to enhance the clonogenic potential of primary mouse bone marrow cells, and affects AML1/ETO's activity on several endogenous genes. Oligomerization is also required for AML1/ETO's interactions with ETO, MTGR1, and MTG16, but not with other corepressor molecules.

Introduction

AML1/ETO is the fusion protein resulting from the t(8;21) found in acute myeloid leukemia (AML) of the M2 subtype (Miyoshi et al., 1993). AML1/ETO contains the N-terminal 177 amino acids of RUNX1 fused in frame with most (575 aa) of ETO. RUNX1 (AML1) is the sequence-specific DNA binding subunit of a core binding factor that is required at multiple stages of hematopoiesis (Growney et al., 2005; Ichikawa et al., 2004; Okuda et al., 1996; Wang et al., 1996). The Runt domain of RUNX1, which is retained in AML1/ETO, mediates DNA binding as well as heterodimerization with the core binding factor β (CBFβ) subunit. ETO (eight twenty-one) was originally identified as the RUNX1 fusion partner in t(8;21), and many of its biochemical properties have been characterized in light of its role in leukemogenesis. The function of ETO itself is less well understood, although its *Drosophila* homolog, Nervy, was recently shown to interact directly with the transcription factor daughterless, and to repress the activity of enhancers normally activated by the achaete-scute complex in the sensory organ precursor cell (Wildonger and Mann, 2005). Homozygous disruption of ETO in mice results in a gastrointestinal defect, but no hematopoietic deficiencies were reported (Calabi et al., 2001). A second ETO family member, MTG16, was purified as part of a complex of transcription factors by virtue of their association with the hematopoietic-specific SCL protein (Schuh et al., 2005). MTGR1, the third member of the mammalian ETO family, is required for the maintenance of secretory epithelial cells in the small intestine (Amann et al., 2005). *MTG16* is also translocated to *RUNX1* in human leukemia (Gamou et al., 1998), potentially underscoring the importance of sequences that are conserved between the ETO proteins for their oncogenic properties.

ETO shares four regions of homology with Nervy (NHR1-4), all four of which are retained in AML1/ETO (Davis et al., 2003; Hug and Lazar, 2004). NHR1 is homologous to several TATA binding protein-associated factors (TAFs) and interacts with E proteins (Zhang et al., 2004). NHR2 is often referred to as the hydrophobic heptad repeat (HHR) because its amino acid sequence is

SIGNIFICANCE

Chromosomal rearrangements often result in the production of chimeric proteins with altered function. In a number of cases, aberrant oligomerization of kinases or transcription factors through the addition of oligomerization domains contributes substantially to the oncogenic potential of these chimeric proteins. Here, we present the three-dimensional structure of the oligomerization domain (NHR2) from ETO, which becomes fused to the AML1 protein as a result of the 8;21 translocation. We show that NHR2 is a tetramer. We also rigorously demonstrate that oligomerization through the NHR2 domain is essential for AML1/ETO's effects on the differentiation and enhanced clonogenic potential of primary bone marrow cells and discuss why it will be difficult to develop small molecule inhibitors of tetramer formation for treating t(8;21) leukemia.

Table 1. Statistics of data collection and refinement

Data statistics[a]			
Wavelength (Å)	0.97946 inflection	0.97915 peak	0.96422 remote
Resolution range (Å)	50.0–2.0	50.0–2.0	50.0–2.0
Total number of reflections	143610	233291	106989
Unique reflections	10199	10096	9499
*R_{merge}	0.026 (0.195)	0.044 (0.196)	0.037 (0.233)
**Anomalous R_{merge}	0.020 (0.172)	0.021 (0.175)	0.020 (0.211)
*Completeness (%)	98.6 (93.8)	99.7 (100.0)	91.9 (92.8)
**Anomalous completeness (%)	96.4 (89.8)	99.7 (99.8)	84.7 (80.5)
**Anomalous average redundancy	2.4 (2.0)	3.6 (3.2)	1.8 (1.8)
Average I/σ(I)	27.0 (6.4)	24.9 (5.5)	20.1 (4.5)
Refinement statistics[b]			
Resolution (Å)	40.0–2.0		
Unique reflections	9346 (645)		
R (%)	21.6 (22.6)		
R_{free} (%)	27.0 (33.7)		
No. non-H protein atoms	1099		
No. water molecules	59		
R.m.s.d. bond lengths (Å)	0.021		
R.m.s.d. bond angles (°)	2.794		
R.m.s.d. torsion angles (°)	6.186		
Average B factor (Å^2)	32.0		
Ramachandran plot			
Residues in most favored region (%)	97.4		
Residues in additional allowed regions (%)	2.6		

[a]Data for the highest resolution shells are in parentheses: peak (2.07–2.00 Å), inflection, and remote (2.06–2.00 Å). *Friedel mates merged. **Friedel mates separated.
[b]Data for the highest resolution shell (2.05–2.00 Å) are given in parentheses.

indicative of an amphipathic helical structure (Lutterbach et al., 1998a). NHR2 contributes many of the most well-studied biochemical properties of ETO, including oligomerization and protein-protein interactions (Amann et al., 2001; Hildebrand et al., 2001; Lutterbach et al., 1998a; McGhee et al., 2003; Zhang et al., 2001). NHR3 is a predominantly α-helical domain (Yang et al., 2004) that interacts with the regulatory subunit of type II cyclic AMP-dependent protein kinase (PKA RIIα) (Fukuyama et al., 2001); however, its contribution to AML1/ETO function may be cooperative with adjacent domains (Hildebrand et al., 2001). NHR4, also known as the myeloid-Nervy-DEAF-1 (MYND) domain, has two putative, non-DNA binding zinc fingers. Like NHR2, NHR4 mediates protein-protein interactions thought to be important for leukemogenesis (Gelmetti et al., 1998; Lutterbach et al., 1998a; Wang et al., 1998).

The NHR2 domain mediates interactions with ETO family members, oligomerization of AML1/ETO, and interactions with mSin3A, Gfi-1, BCL6, and HDAC1 and HDAC3 (Hiebert et al., 2001; Hug and Lazar, 2004). The generation of oligomeric transcription factors by translocation partner sequences is emerging as a common transforming mechanism in many hematological malignancies (So and Cleary, 2004). It has been proposed that oligomerization generates a surface required for high-affinity corepressor interactions, and in the case of AML1/ETO, oligomerization was shown to augment SMRT interaction in vitro (Zhang et al., 2001). Here, we present the crystal structure of the isolated NHR2 domain. NHR2 forms a four-helix bundle tetrameric structure stabilized by an extensive hydrophobic interface contributed by the four amphipathic α helices and specific intersubunit electrostatic interactions. We introduced amino acid substitutions into NHR2 with the goal of disrupting oligomerization while maintaining solubility and minimally compromising the helical secondary structure, and confirm that oligomerization is critical for AML1/ETO function in vivo.

Results

Structure determination

We crystallized the SeMet substituted NHR2 domain (residues 480–551, AML1/ETO numbering), collected diffraction data from a single crystal at three wavelengths (0.97915 Å [peak], 0.97946 Å [inflection], and 0.96422 Å [remote]), and solved the structure at 2.0 Å resolution by multiple wavelength anomalous dispersion (MAD). We traced residues 490–548 in both protein chains but observed no continuous electron density that could be used for model building for residues 480–489 and 549–551. Details of data collection and structure determination are summarized in Table 1. The coordinates and structure factors are deposited in the Protein Data Bank with accession code 1WQ6.

The asymmetric unit contains two molecules (Figure 1A) related by an "approximate" 2-fold noncrystallographic symmetry (backbone r.m.s.d.: 0.97 Å). Each polypeptide chain consists of one long curved α helix (Asp495–Ala547) with a kink at Ile512. The homotetrameric model is established by rotating the asymmetric unit around the 2-fold axis of the $P2_12_12$ space group (Figure 1A). The two antiparallel molecules in the asymmetric unit are aligned at 173.6° in a head-to-tail fashion and lie on top of the other antiparallel pair (Figure 1B: C3 and C4) at a 21° angle to form a left-handed supercoil. Indeed, the NHR2 primary sequence displays the 7-residue repeat characteristic of left-handed coiled coils (Antonin et al., 2002; Harbury et al., 1993) (Figure 2A). The monomer is amphipathic and interacts with the other three monomers through hydrophobic interactions that bury a total accessible surface area (ASA) of 10,645 Å^2

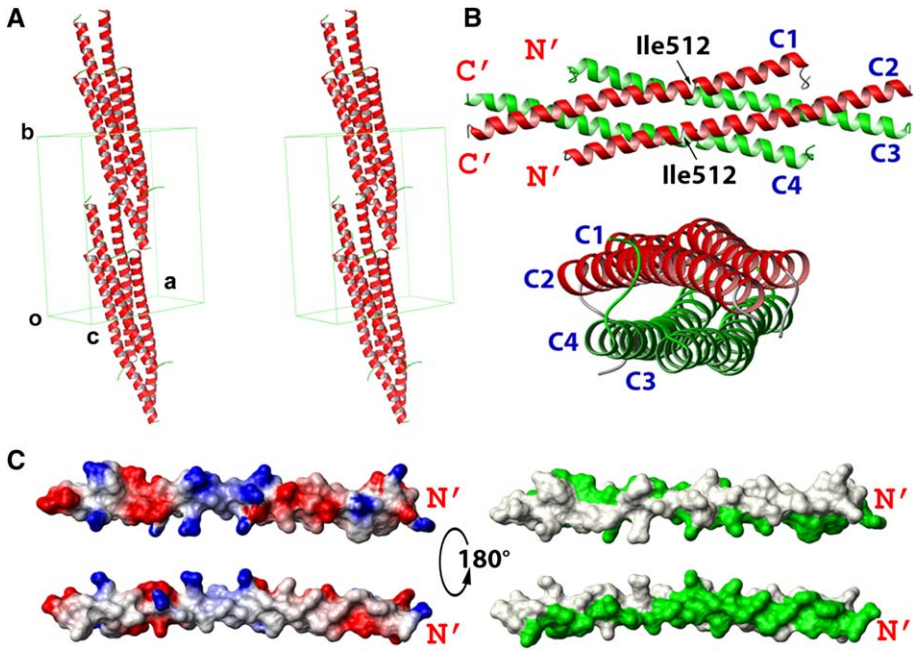

Figure 1. Structure of the NHR2 domain

A: Unit cell packing: there are four half tetramers per unit cell. Only two halves are shown for clarity. Lowercase a, b, and c denote the unit cell axes.

B: Ribbon representation of the tetramer in two different orientations. The four chains in the tetramer are labeled C1, C2, C3, and C4. The asymmetric unit can be chosen so that it contains C1 and C2 (red). C3 and C4 (green) are related to C1 and C2 by crystallographic symmetry. The kink at Ile512 is indicated. N′ and C′ denote the N and C termini.

C: Surface views of a single molecule (C1). Electrostatic distribution on the two sides of the amphipathic helix is shown on the left, with positively charged (blue), negatively charged (red), and uncharged (ivory) atoms indicated. Right: distribution of solvent-accessible surface area on the two sides of the amphipathic helix. Residues with >50% of their solvent-accessible surface area buried in the tetramer are shown in green. N′ denotes the N terminus.

(average of 2661 Å^2 per monomer). The large contact area is consistent with oligomerization rather than crystal contacts. The tetrameric structure was predicted by PITA (protein interactions and assemblies) (Ponstingl et al., 2000) and confirmed in solution by analytical ultracentrifugation (Table 2).

The tetramer forms an interaction motif through hydrophobic heptad repeats and ionic/polar interactions

The NHR2 tetramer contains an N-terminal tetrameric region with ten symmetrical interacting layers (−5 to −1 and 1 to 5) and two symmetrical C-terminal dimeric regions with five interacting layers (e′–a′ and a–e) (Figure 2A). This unusual interaction pattern occurs as a result of the indented alignment of the antiparallel molecules and the relatively small intersection angle (21°) between the two dimers. To the best of our knowledge, such an interaction motif has not been reported previously. Most of the layers consist of hydrophobic residues at the "a" and "d" positions of the heptad helical wheel (Figures 2A and 3B). The two molecules in the asymmetric unit (C1 and C2, or C3 and C4) display some asymmetry not only in conformation but also in contact surface (Figures 1B and 2D). All the "a" and "d" residues in the tetrameric region of both molecules are more than 90% buried (Figure 2D), and "a" and "d" residues in the dimeric region are more than 65% buried, except for Ala547, which is at the very end of the helix. This is similar to what is observed for the dimeric leucine zipper domain of GCN4 (Harbury et al., 1993). The "e" and "g" residues in the tetrameric region are greater than 60% buried (Figure 2D), consistent with what has been reported for a tetrameric mutant of GCN4: p-LI (Harbury et al., 1993). The hydrophobic core is packed between the four molecules in a sandwich-like fashion (Figure 2C).

A number of polar and charged residues make important stabilizing interactions that are not typically seen in leucine zippers. For example, the Thr519 side chains are buried in layers +2 and −2, and Gln530 is packed in layers +5 and −5 (Figure 2A). The hydroxyl group of Thr519 forms an intramolecular hydrogen bond with the carbonyl group of Met515 (Thr519 Oγ − Met515 CO = 2.8 Å) (data not shown). This type of hydrogen bonding between Thr i and X i-4 has also been observed in the endosomal SNARE complex (Antonin et al., 2002; Fasshauer et al., 1998). In layers +5 and −5, Gln530 of C1 forms a specific intermolecular hydrogen bond with Trp502 of C2 (Gln530 Oε − Trp502 Nε1 = 2.96 Å), while asymmetrically, Gln530 of C4 in the same layer displays an intermolecular hydrogen bond with Leu526 of C1 (Gln530 Nε2 − Leu526 O = 3.11 Å) (Figure 2E).

Two symmetrical groups of intermolecular salt bridge interactions are observed in the tetrameric complex (Figure 2F). One consists of intermolecular interactions between Arg520 and Asp506 that form solvent-exposed salt bridges (Figure 2F). This type of surface ionic interaction was shown to be important for stability in the GCN4 dimer (Spek et al., 1998). The other symmetrical group occurs at layers a and a′ and involves residues at the "a" and "d" positions of the heptad helical wheel. In leucine zipper oligomers, there are buried hydrophobic residues at these locations that contribute to oligomerization, but the NHR2 tetramer instead contains charged residues that form buried salt bridges with good geometry. For example, Asp533 of C2 forms salt bridges with Arg534 of C3 (Figure 2F). Both Asp533 and Arg534 are almost completely buried (Figure 2D), and the highly favorable electrostatic interaction energy offsets the desolvation penalty for burying the charges.

Oligomerization contributes to AML1/ETO's activity

We assessed the importance of oligomerization for AML1/ETO function by introducing amino acid substitutions into NHR2 that disrupt tetramer formation. We sought to achieve three goals when designing the mutations: (1) to disrupt the oligomerization interface, (2) to confer favorable solubility properties to the mutant domain, and (3) to preserve the α-helical secondary structure as much as possible. The Leu residues at the interface contribute substantially to the stability of the tetramer, and

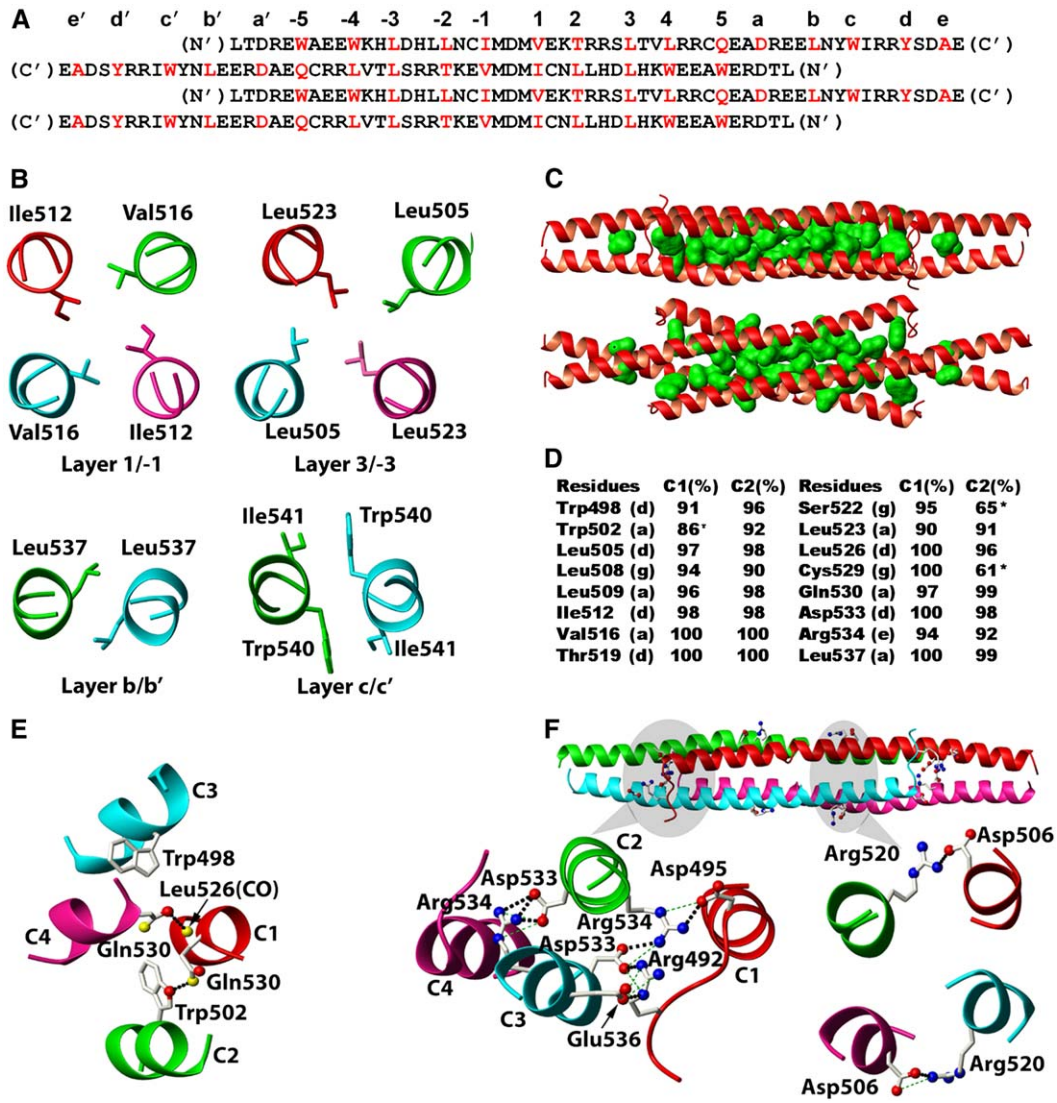

Residues	C1(%)	C2(%)	Residues	C1(%)	C2(%)
Trp498 (d)	91	96	Ser522 (g)	95	65*
Trp502 (a)	86*	92	Leu523 (a)	90	91
Leu505 (d)	97	98	Leu526 (d)	100	96
Leu508 (g)	94	90	Cys529 (g)	100	61*
Leu509 (a)	96	98	Gln530 (a)	97	99
Ile512 (d)	98	98	Asp533 (d)	100	98
Val516 (a)	100	100	Arg534 (e)	94	92
Thr519 (d)	100	100	Leu537 (a)	100	99

Figure 2. Analysis of the NHR2 structure

A: Primary sequence alignment of the NHR2 domain based on the actual topology. Residues occupying the ''a'' and ''d'' positions of the canonical heptad helical wheel are colored red. The ''a'' and ''d'' positions in the tetrameric layers are labeled with numbers (−5 to −1 and 1 to 5) and in the dimeric layers with letters (e′–a′ and a–e). Layers related by opposite signs or primes are strictly symmetrical in the structure.

B: Selected cross-sections of hydrophobic layers. The four molecules are labeled with different colors for clarity.

C: Packing of the hydrophobic core in the tetramer. Residues with >90% of their solvent-accessible surface buried in the tetramer are shown in green.

D: Solvent-accessible surface area for residues that are >90% buried in C1 or C2. The position in the helical wheel is also indicated. Residues with values <90% are indicated with an asterisk.

E: The intermolecular hydrogen bonds at layer +5 involving Gln530, Leu526, and Trp502.

F: Detailed views of two salt-bridged layers. Hydrogen-bonded salt bridges are shown as black dashed lines, and non-hydrogen-bonded salt bridges are shown as green dashed lines (defined as in Kumar and Nussinov, 1999).

therefore we targeted them for mutagenesis. We tried several different substitutions (see Table S1 in the Supplemental Data available with this article online), only two of which significantly disrupted tetramer formation, and which are reported here. The m7 mutant contained Arg and Glu substitutions for the seven Leu residues, with the charged residues placed appropriately for favorable intrahelical electrostatic interactions (Figure 3B). The placement of charge on the interface was designed to disrupt oligomerization and provide favorable solubility properties to the monomeric domain. In addition, both Arg and Glu have a high α-helical propensity, so it was hoped that the monomeric domain would retain some of its α-helical character. The m4 mutant had four Leu residues replaced with Lys, Glu, or Gln (Figure 3B). The three Leu residues at the reported interface for mSin3A (Amann et al., 2001) were not altered in m4. Finally, we substituted two solvent exposed residues (m2, Figure 3B) that were required for mSin3A binding to the isolated NHR2 domain (Amann et al., 2001).

We characterized the solution oligomerization state and secondary structure of the wild-type and mutant NHR2 domains by sedimentation velocity and circular dichroism (CD) spectroscopy, respectively. Figure 3C shows that the continuous

Table 2. Analysis of NHR2 oligomerization by sedimentation velocity[a]

Protein	Mass (kDa)	s (svedbergs)	% Contribution[b]	r.m.s.[c]
NHR2[d]	36.1	2.68	91	0.0069
m7[e]	7.6	1.09	92	0.0117
m4[d]	33.3	2.85	84	0.0109
m2[f]	34.2	2.71	91	0.0053

[a]Sedimentation profiles obtained at two to three loading concentrations were globally analyzed with SEPHAT using a hybrid discrete-continuous distribution model to obtain the mass and sedimentation coefficient of the majority species for each protein.
[b]The weight percent contribution of the majority species was obtained by integration of a continuous sedimentation coefficient distribution function from ~1.9 to ~3.5 S with SEDFIT. Large aggregates with s > 100 S were observed in several samples and were not included in the analysis.
[c]Root mean square deviation of the global fit in units of OD (absorbance) or fringes (interference).
[d]Data obtained at 0.6, 0.3, and 0.1 mg/ml using absorbance at 280 nm.
[e]Data obtained at 0.2, 0.09, and 0.05 mg/ml using absorbance at 230 nm. Approximately 30%–45% of the material sedimented with s > 100 S.
[f]Data obtained at 0.15, 0.09, and 0.05 mg/ml using absorbance at 230 nm. Approximately 25% of the material sedimented with s > 100 S.

sedimentation coefficient distribution for NHR2 contains a major peak near s = 2.7 S, corresponding to 91% of the material. The molecular mass of this predominant species is 36.1 kDa (Table 2) which corresponds closely to the predicted tetramer mass of 35.8 kDa. Thus, the NHR2 domain is clearly a tetramer in solution. Hydrodynamic modeling using the crystal structure predicts a sedimentation coefficient of 2.87 S, which agrees well with the experimental value of 2.68 S.

The sedimentation coefficient of m7 was ~1.1 S and the mass 7.6 kDa, indicating that m7 is a soluble monomer (Figure 3C and Table 2). CD spectroscopy indicates that the percentage of residues with helical secondary structure was reduced from 60% in NHR2 to 17% in the m7 mutant (Figure 3D). The m4 mutant was tetrameric at 20ºC by analytical ultracentrifugation (Table 2), but CD spectroscopy revealed that it was only 41% helical, suggesting that the m4 tetramer is significantly destabilized. We characterized the stability of m4 more extensively by thermal denaturation and renaturation experiments monitored by CD spectroscopy. The NHR2 domain unfolds with a sharp transition at a melting temperature >90ºC (Figure S1), indicative of the extremely high stability of the tetramer. In contrast, m4 unfolding occurs with a broad transition and a midpoint around 50ºC; therefore, the m4 tetrameric structure should be destabilized at physiological temperatures. The m2 domain is tetrameric and has a similar sedimentation coefficient (Table 2) and CD spectrum (Figure 3D), and therefore similar structure as the NHR2 domain.

We deleted the NHR2 (Figure 3A) and introduced the m7, m4, and m2 mutations into full-length AML1/ETO and assessed their effect on oligomerization by size exclusion chromatography (SEC) (Figure 3E). As shown by others (Minucci et al., 2000; Zhang et al., 2001), full-length AML1/ETO (84 kDa) migrates with an apparent molecular mass greater than 400 kDa. Deletion of the NHR2 domain (Zhang et al., 2001), the m7 mutation, and the m4 mutation shifted the migration of AML1/ETO to that of lower-molecular weight species (Figure 3E). Consistent with the sedimentation velocity and CD measurements, the m4 version of AML1-ETO shows an elution volume intermediate between m7 and AML1-ETO. The m2 mutation did not affect the SEC elution profile (data not shown).

We used retroviruses to introduce AML1/ETO and its mutated derivatives into lineage-depleted ($CD5^-$, $B220^-$, $Mac\text{-}1^-$, $Gr\text{-}1^-$, $Ter119^-$) mouse bone marrow cells (Lin^- BM) in order to assess the importance of oligomerization for AML1/ETO function. The retroviruses also expressed the green fluorescent protein (GFP) from an internal ribosome entry site, allowing us to monitor successfully transduced cells. We cultured the transduced cells for 2 days in the presence of IL-3, IL-6, and SCF, and for 7 additional days with the same cytokines plus G-CSF to induce granulocyte differentiation, and analyzed GFP^+ cells for cell surface Gr-1 and Mac-1 expression (Figure 4A). Approximately 20% of Lin^- BM cells expressing GFP alone were $Gr\text{-}1^+$ $Mac\text{-}1^+$, whereas only 3% of cells expressing AML1/ETO differentiated into $Gr\text{-}1^+Mac\text{-}1^+$ cells. As shown by Hug et al. (2002), deletion of the NHR2 domain partially impaired AML1/ETO's repression of granulocyte differentiation, resulting in a 3-fold increase in the percentage of $Gr\text{-}1^+Mac\text{-}1^+$ cells. The m7 mutation increased the percentage of $Gr\text{-}1^+Mac\text{-}1^+$ cells to the same extent as the NHR2 deletion. The m4 mutation impaired AML1/ETO's activity, but significantly less so than the NHR2 deletion. The m2 mutation had no effect on AML1/ETO's ability to repress granulocyte differentiation.

An AML1/ETO protein truncated at aa 542, C-terminal to the NHR2 domain (NHR2x; Figure 3A) partially inhibits the differentiation of $Gr\text{-}1^+Mac\text{-}1^+$ cells, and the m7 mutation in the context of this truncated NHR2x protein (NHR2x m7) completely abrogates AML1/ETO's activity (Figure 4A). All of the mutated proteins accumulated to similar steady-state levels in retrovirus-infected NIH 3T3 cells despite the fact that the m4 and m7 mutations partially destabilized NHR2's helical structure (Figure 4B).

Disruption of oligomerization abrogates AML1-ETO's ability to promote self-renewal

We assessed the importance of tetramer formation for AML1/ETO's ability to confer increased self-renewal capacity on hematopoietic progenitors in vitro (Higuchi et al., 2002; Hug et al., 2002; Mulloy et al., 2002). Lin^- BM cells were infected with retroviruses expressing AML1/ETO and its mutated derivatives and cultured in IL-3, IL-6, and SCF. Cells expressing AML1/ETO could be propagated for at least 3 weeks in culture and yielded primarily immature myeloid lineage cells (Figures 4C and 4D) and a smaller percentage of differentiated macrophages (data not shown). In contrast to the results of Hug et al. (2002), we found that deletion of NHR2 completely abolished AML1/ETO's ability to sustain clonogenic activity in vitro, as did the m7 and m4 mutations (Figure 4C). Mutation of the mSin3A binding site in NHR2 (m2), however, had no effect on AML1/ETO's ability to confer enhanced clonogenic potential (Figure 4C). Truncation of AML1/ETO at the C terminus of NHR2 (NHR2x) eliminated AML1/ETO's clonogenic activity, despite the observation that a similar construct retaining 9 additional amino acids and a terminal four-residue insertion was shown to augment AML1/ETO's leukemogenic activity in mice (Yan et al., 2004).

Disruption of AML1/ETO oligomerization alters endogenous gene expression

We transduced Lin^- BM cells with retroviruses expressing GFP alone, AML1/ETO, or m7 and assessed the expression levels of candidate target genes 2 days posttransduction by real-time

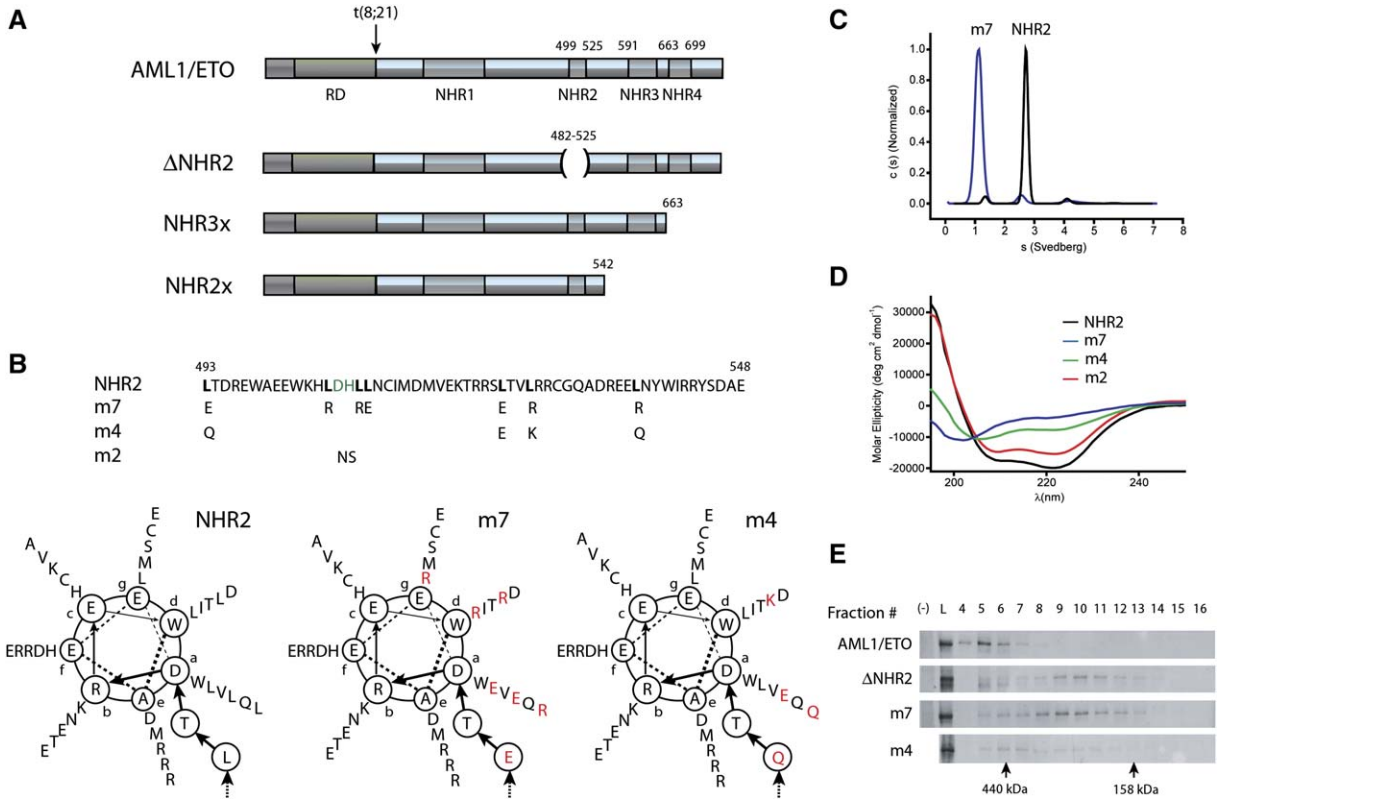

Figure 3. Mutations in the NHR2 domain and their effect on tetramer formation

A: Schematic diagram of AML1/ETO. The Runx1 (AML1) portion is green, and ETO sequences are blue. Truncations and internal deletions used in the analyses are shown below. Parentheses in ΔNHR2 delineate the extent of the deletion. RD, Runt domain.

B: Sequence of the NHR2 domain (Leu in bold, the two amino acids required for mSin3A binding [Amann et al., 2001] in green) and the mutations designed to disrupt tetramer formation (m7 and m4) and mSin3A binding (m2). Diagramed below are the m7 and m4 mutations in NHR2 in a helical wheel representation. Substituted amino acids are red.

C: Sedimentation velocity analysis of NHR2 and the m7 mutant. Absorbance data at 280 nm (NHR2) and 230 nm (m7) were collected at a rotor speed of 50,000 rpm at 20°C in aluminum-filled Epon double sector cells at a scan interval of approximately 260 s.

D: Circular dichroism spectroscopy of NHR2 domains (recorded at 25°C). The reduction in ellipticity at 222 nm for m7 and m4 is indicative of a loss of helical secondary structure.

E: Size exclusion chromatography (SEC) demonstrating that deletion of the NHR2 domain and the m7 and m4 mutations reduces the apparent molecular weight of full-length AML1/ETO. Proteins were produced by in vitro transcription/translation and fractionated by SEC on a Superdex 200 column, and fractions were analyzed by Western blot using an anti-Runt domain antibody. Fraction numbers are indicated above lanes, and molecular weight markers are on the bottom. (−), reticulocyte lysate incubated with the pcDNA vector; L, load.

PCR (Figures 5A–5D). Genes that were analyzed were either previously implicated as Runx1 or AML1/ETO targets (Elagib et al., 2003; Otto et al., 2003; Peterson and Zhang, 2004) or identified based on hybridization to pathway-specific microarrays (data not shown). Other labs have reported that AML1/ETO expression activates some genes and represses others (Shimada et al., 2000, 2002), and we likewise observed several different patterns resulting from AML1/ETO and m7 expression. Some genes previously shown to be activated by Runx1, including *Art1*, *Csf1r* (MCSFR), *Ela2* (neutrophil elastase [NE]), and *Sfpi1* (PU.1) (Otto et al., 2003; Peterson and Zhang, 2004) were repressed in Lin^- BM cells transduced with AML1/ETO, and the m7 mutation restored their expression to the levels observed in cells expressing GFP alone (Figure 5A). The cell cycle gene *E2f2* and the *Jak2* kinase gene also fell into this category. A second pattern seen with *Itga2b* (CD41), *Mpo*, and *Ccnd3* (CycD3) was that AML1/ETO had no significant effect, while m7 activated their expression (Figure 5B). These three genes were previously shown to be direct (activated) targets of Runx1. A third pattern seen with *Fos* (c-fos), the *Cd53* tetraspanin gene, and *Cdkn1a* (p21) was activation by AML1/ETO, with blunting of that activation by the m7 mutation (Figure 5C). Finally, expression of neither the putative AML1-ETO target gene *Bcl2*, nor *Bmi1* was significantly altered in the presence of either AML1/ETO or m7 (Figure 5D).

AML1/ETO's interaction with members of the ETO family of proteins, but not with other corepressors, requires oligomerization

AML1/ETO has been shown to interact directly or indirectly with a number of other proteins, including HDAC1, HDAC2, and HDAC3, N-CoR, SMRT, mSin3A, Gfi-1, BCL6, PLZF, PKA RIIα, HEB, and other ETO family members (Hiebert et al., 2001; Hug and Lazar, 2004). We examined whether oligomerization through the NHR2 domain affects the direct or indirect association of AML1/ETO-interacting proteins in vivo. FLAG- or HA-tagged versions of interacting proteins were coexpressed with either HA-tagged or untagged versions of AML1/ETO or

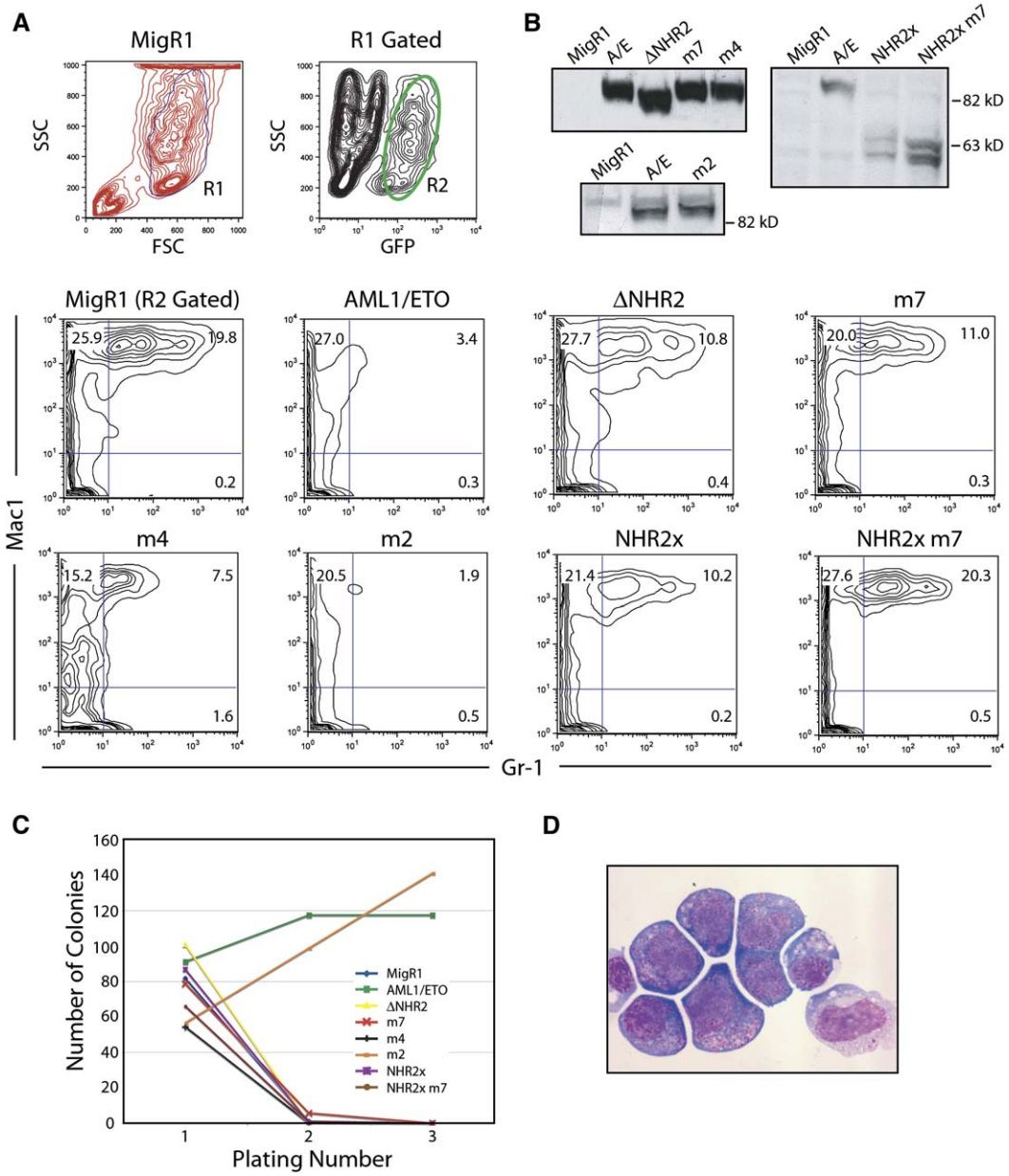

Figure 4. AML1/ETO function is impaired by mutations that disrupt tetramer formation, but not by mutations in the mSin3A binding site

A: Representative flow of Lin$^-$ BM cells infected with MigR1 retroviruses expressing AML1/ETO and mutated derivatives, following 7 days of culture in the presence of IL-3, IL-6, SCF, and G-CSF. Cells in the R1 gate were analyzed for GFP expression, and GFP-positive cells (R2) were examined for Mac-1 and Gr-1 expression. The experiments were performed at least twice with triplicate samples. The average percentages of Gr-1$^+$Mac-1$^+$ cells (± standard deviation) in the illustrated experiments were as follows. Experiment #1: MigR1 (GFP alone), 19.3% (1.1); AML1/ETO, 3.6% (0.2); ΔNHR2, 10.8% (1.0); m7, 8.9% (1.0); m4, 7.5% (0.3). The difference between m7 and m4 versus AML1/ETO was significant ($p \leq 0.01$). m7 was not significantly different from ΔNHR2 or m4. m4 was significantly different from ΔNHR2 ($p \leq 0.05$). Experiment #2: MigR1, 15.6% (2.1); AML1/ETO, 1.5% (0.1); m2, 1.8% (0.1). m2 and AML1/ETO were not significantly different. Experiment #3: MigR1, 22.4% (5.0); AML1/ETO, 3.1% (0.7); NHR2x, 9.2% (1.1); NHR2x m7, 19.1% (1.5). The difference between MigR1 and NHR2x m7 was not significant.

B: Western blot probed with an antibody to the Runt domain, demonstrating expression of AML1/ETO and its mutated derivatives in MigR1-transduced NIH3T3 cells.

C: Serial replating of bone marrow cells. Graphs represent the average number of colonies from each round of replating in the presence of IL-3, IL-6, and SCF. Plating number 1 represents colony numbers per 10^3 cells plated, and plating numbers 2 and 3 are from 10^4 plated cells. Numbers are averaged from two experiments, each containing triplicate samples. The average numbers of cells (± SD) at week three of replating are as follows: AML1/ETO, 117 (9.5); m2, 141 (26). The other cultures had no cells at 3 weeks.

D: Cytospin preparation of cells expressing AML1/ETO from the third replating. The majority of cells (~85%) were immature myelocytes or monocytes, and the remainder were primarily macrophages (data not shown). Only a few mature granulocytes were visible (data not shown).

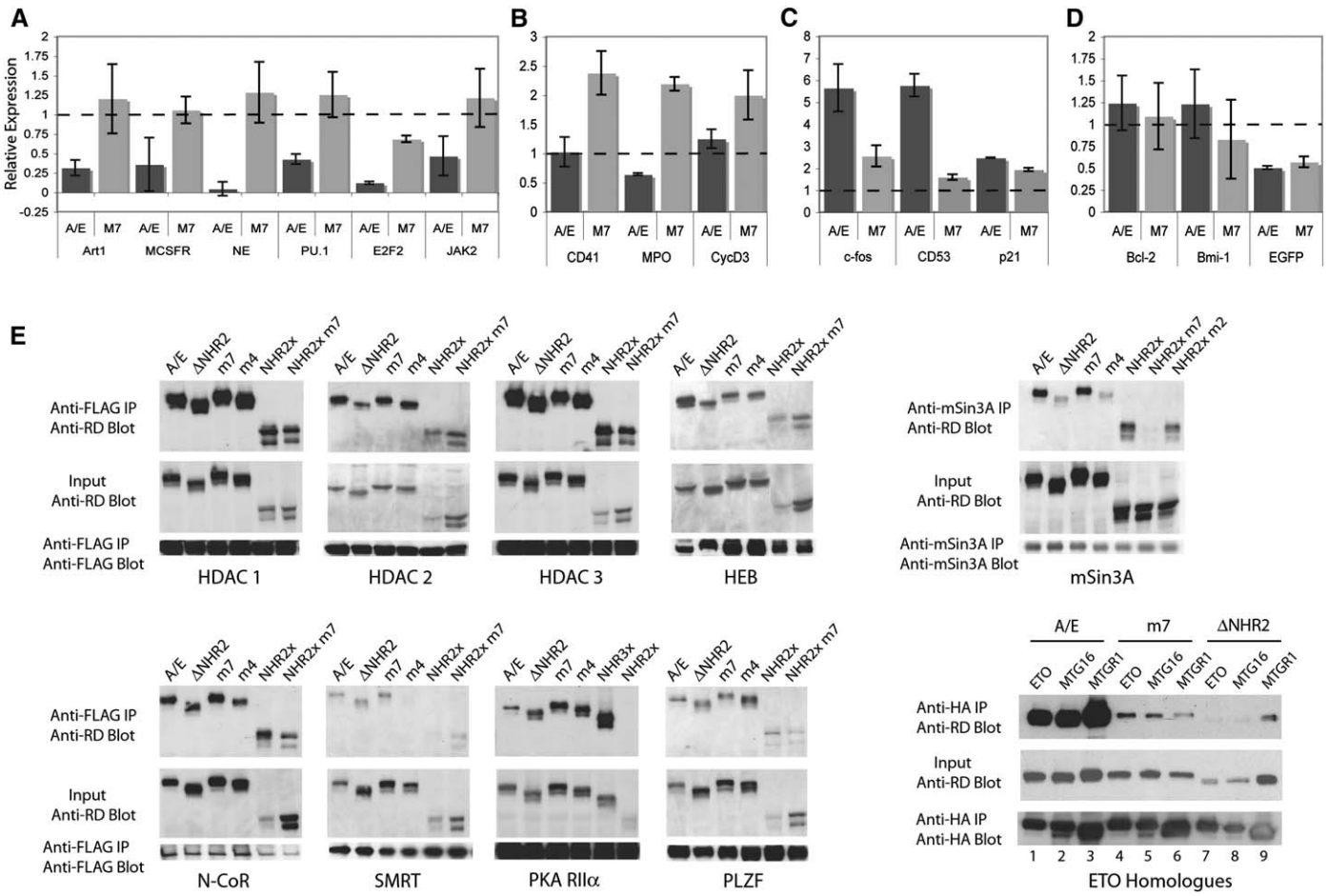

Figure 5. Oligomerization influences AML1/ETO's regulation of gene expression, but not its association with interacting proteins, with the exception of ETO, MTG16, and MTGR1

A–D: Real time PCR of putative Runx1 or AML1/ETO target genes in Lin$^-$ BM cells to assess the role of oligomerization in gene expression. Gene expression data are presented as the fold change between control EGFP-transduced cells (normalized to a value of 1, dashed line) and AML1/ETO or m7-transduced cells and represent averages from three independent experiments. Error bars indicate 95% confidence intervals. **A:** Genes whose expression is repressed in the presence of AML1/ETO and m7 restores expression to that of EGFP alone. **B:** Genes activated by m7 but not AML1/ETO. **C:** Genes activated by AML1/ETO and less so by m7. **D:** Examples of genes whose expression is not affected by either AML1/ETO or m7. The 2-fold reduction in EGFP expression, which was equivalent for AML1/ETO and m7, was most likely due to its translation from bicistronic (AML1/ETO and m7) versus monocistronic (EGFP alone) mRNAs.

E: Cos7 cells were cotransfected with HA-tagged (AML1/ETO [A/E] and m7) or nontagged (ΔNHR2, m4, NHR3x, NHR2x, NHR2x m7, NHR2x m2) AML1/ETO proteins and FLAG-tagged HDAC1, HDAC2, HDAC3, N-CoR, SMRT, PKA RIIα, or HEB. For experiments involving ETO homologs, cells were transfected with HA-tagged ETO, MTG16, and MTGR1 and untagged AML1/ETO. Top panels: cell lysates immunoprecipitated (IP) with anti-FLAG or anti-HA antibody and blotted with antibody to the Runt domain (RD) in AML1/ETO. The interaction between mSin3A and transfected AML1/ETO proteins was analyzed by immunoprecipitating endogenous mSin3A and blotting with the anti-RD antibody. Middle panels: 1% of input lysate, blotted with anti-RD to detect AML1/ETO proteins. Bottom panels: membranes from the top panel were reprobed with anti-FLAG, anti-HA, or anti-mSin3A antibodies. The percentages of input AML1/ETO and m7 proteins in the immunoprecipitates were determined by titration analyses and were as follows: HDAC1, 1.5 and 1.4 (AML1/ETO and m7, respectively); HDAC2, 0.7 and 0.7; HDAC3, 1.3 and 1.3; mSin3A, 0.6 and 0.3; N-CoR, 0.8 and 0.7; SMRT, 0.9 and 0.9; PKA RIIα, 1 and 1; PLZF, 0.8 and 0.7, HEB, 1 and 0.4. ETO homolog immunoprecipitates were not quantified.

its mutated derivatives in Cos7 cells, and their interactions were monitored by coimmunoprecipitation (Figure 5E). The interaction of AML1/ETO with endogenous mSin3A was also examined. We found that deletion of the NHR2 domain weakened full-length AML1/ETO's interactions with mSin3A, to some extent with HDAC2, and dramatically affected interactions with all of the ETO family proteins (ETO, MTG16, and MTGR1). However, when AML1/ETO oligomerization was specifically disrupted by the m7 mutation, only the interactions with ETO, MTG16, and MTGR1 were markedly affected. The m7 mutation in the context of an AML1/ETO protein truncated at the C terminus of the NHR2 domain (NHR2X versus NHR2Xm7) did disrupt binding to mSin3A and may have weakened the interaction with N-CoR, but it did not noticeably or consistently affect the efficiency of coimmunoprecipitation with the HDACs, HEB, SMRT, or PLZF. m4 weakened full-length AML1/ETO's interaction with mSin3A and almost completely abrogated its ability to coimmunoprecipitate with SMRT, but since m4 did not disrupt oligomerization to the same extent as m7, the weakened binding to mSin3A and SMRT was not specifically caused by the loss of oligomerization. In summary, although AML1/ETO's in vivo activity is dependent on oligomerization, its binding to

the ectopically expressed corepressor proteins, with the exception of the ETO family of proteins, was not appreciably affected by mutations that specifically impair oligomerization.

Discussion

Oligomerization is important for the oncogenic potential of a number of leukemia-associated chimeric proteins. This phenomenon was originally documented for the BCR/ABL kinase (McWhirter et al., 1993), and in transcription factors was first observed for fusion proteins involving the retinoic acid receptor α (RARα) (Lin and Evans, 2000; Minucci et al., 2000). Since these initial observations, an in vivo role for oligomerization has been documented for chimeric transcription factors containing RUNX1 (AML1/ETO, AML1/MTG16, TEL/AML1), CBFβ (CBFβ/SMMHC), RARα (NPM/RARα, PML/RARα, PLZF/RARα, NuMA/RARα, Stat5b/RARα), and MLL (MLL/GAS7, MLL/AF1p, MLL/GEPHRIN), which together account for a high percentage of leukemia cases (Eguchi et al., 2004; So and Cleary, 2004). The paradigm for the effects of aberrant oligomerization on transcription factor function is the fusion of RARα to PML and PLZF in acute promyelocytic leukemia, which affects RARα's in vivo function and its binding to the corepressors N-CoR and SMRT (Melnick and Licht, 1999).

The NHR2 domain of ETO is also an oligomerization domain, and it is important for AML1/ETO's activity. Our structural results show that NHR2 forms a homotetrameric α-helical bundle with a left-handed supercoil resembling the structure found in the heterotrimeric SNARE complexes (Sutton et al., 1998). We used the NHR2 structure to design mutations that disrupted oligomerization but conferred favorable solubility properties to the domain and preserved a significant proportion of its secondary structure. Unlike a deletion, the mutations we employed do not create artificial restrictions on the relative positioning of other domains and may retain some of the protein-protein interactions mediated by the NHR2 domain. Mutations designed to disrupt oligomerization were introduced into full-length AML1/ETO to determine which biological and biochemical properties previously ascribed to oligomerization through deletion studies can actually be attributed to oligomerization per se. Our results confirm the importance of oligomerization for the activity of AML1/ETO in hematopoietic differentiation, proliferation, and gene expression assays (Hug et al., 2002; Shimada et al., 2000; Zhang et al., 2001). Disrupting oligomerization partially impaired AML1/ETO's inhibition of granulocyte differentiation, completely ablated its ability to enhance the clonogenic capacity of primary hematopoietic progenitors, and affected its ability to influence the expression of endogenous genes in primary bone marrow stem and progenitor cells.

We also assessed the outcome of disrupting oligomerization on previously described protein-protein interactions. Eliminating oligomerization impaired AML1/ETO's ability to interact, presumably through tetramerization, with ETO and its homologs MTG16 and MTGR1, as shown previously with an NHR2 deletion (Kitabayashi et al., 1998). MTG16 is found in complexes in hematopoietic cells containing other transcription factors such as SCL, E12/E47, E2.2, Lbd-1, SSDP2, GATA-1, Gfi-1, and LMO2 (Schuh et al., 2005). If AML1/ETO's activity in leukemia is exerted, in part, through complexes containing MTG16, disrupting its ability to form mixed tetramers with MTG16 could potentially interfere with its activity, a hypothesis previously advanced by others (Amann et al., 2001).

Oligomerization was not required for HDAC1, HDAC2, HDAC3, N-CoR, SMRT, PKA RIIα, PLZF, mSin3A, or HEB to coimmunoprecipitate AML1/ETO from cell extracts. Hiebert and colleagues reported that an NHR2 deletion reduced, but did not eliminate AML1/ETO (or ETO) binding to mSin3A, N-CoR, or the HDACs (Amann et al., 2001; Lutterbach et al., 1998a, 1998b). With a more precise oligomerization mutant, we did not see a reduction in AML1/ETO binding to these proteins, except for mSin3A and N-CoR in the context of a truncated AML1/ETO protein. This is not to say that interaction with corepressors is not important for AML1/ETO's activity, only that oligomerization does not appear to be contributing to AML1/ETO's activity by increasing its affinity for these proteins. Oligomerization could, however, increase the number of corepressors recruited to the DNA without altering affinity. A tetramer of AML1/ETO (or a mixed tetramer consisting of AML1/ETO and other ETO homologs) would have the potential to recruit 4-fold more repressor molecules to the DNA than monomeric AML1/ETO, thereby increasing the local concentration of corepressors on target genes. Another possible mechanism by which oligomerization might contribute to AML1/ETO's activity is by augmenting DNA binding, particularly to enhancers and promoters that contain multiple Runx binding sites, allowing it to effectively compete with the normal core binding factors for occupancy. A model for this is the enhanced occupancy of *Hox a9* by dimerized forms of MLL (Martin et al., 2003). Establishing cell lines expressing equivalent amounts of AML1/ETO and m7 will be necessary to test these various models by chromatin immunoprecipitation assays.

Disruption of oligomerization in AML1-ETO resulted in clear changes in the expression of a number of endogenous genes that have been implicated in the development of leukemia or myeloproliferative disorders. Some genes were positively and others negatively regulated by AML1/ETO, as has been observed by others (Shimada et al., 2000, 2002). Some genes may be direct and others indirect AML1/ETO targets, which could account for these seemingly opposite activities. The most intriguing differentially regulated target is the *Sfpi1* gene that encodes PU.1, a transcription factor critical for normal myeloid development (McKercher et al., 1996; Scott et al., 1994). Reductions in PU.1 dosage were recently shown to cause an accumulation of c-kit$^+$ hematopoietic precursors in bone marrow, and predisposed mice to acute myeloid leukemia and T cell lymphoma (Rosenbauer et al., 2004, 2006). AML1/ETO is also thought to inhibit the transcriptional activity of the PU.1 protein, and expression of PU.1 in t(8;21) containing Kasumi-1 cells promoted their differentiation (Vangala et al., 2003). AML1/ETO's ability to reduce both PU.1 dosage and function could be critical for establishing the preleukemic state.

Since disrupting tetramer formation ameliorates some of AML1/ETO's deleterious in vivo effects, an obvious question is whether the tetramer interface is a good target for small molecules or peptides that inhibit oligomerization. We predict that the extremely stable nature of the tetramer, reflected in both its thermal stability and the extensive mutagenesis necessary to disrupt its formation, would make developing small molecule inhibitors of this interaction quite challenging. A more promising approach might be to disrupt the interaction between AML1/ETO and the coregulatory molecules important for its activity.

Identifying which of these molecules is critical for oligomeric AML1/ETO's oncogenic activity is an important area of investigation.

Experimental procedures

Cloning, expression, and protein purification

Cloning, expression, and protein purification were carried out according to standard procedures (details provided in Supplemental Data). FLAG-tagged mammalian expression constructs for HDAC1–HDAC3, N-CoR, and SMRT, and HA-tagged ETO, MTG16, and MTRG1, were generous gifts from Scott Hiebert. N-terminal FLAG tags were added to PKA RIIα, HEB, and PLZF using PCR, and the resulting constructs were cloned into pcDNA3.1(+).

Crystallization

The Se-Met labeled NHR2 domain (AML1/ETO residues 480–551) was dialyzed into 25 mM Tris (pH 7.5), 15 mM NaCl, and 1 mM DTT and concentrated to 10 mg/ml. The protein was mixed 1:1 with well solution (100 mM NaCit [pH 5.6], 100 mM $MgCl_2$, 40% MPD [2-methyl-2,4-pentanediol]) and crystallized by sitting drop vapor diffusion. Crystals reached their full size in 3–4 days. Crystals were removed from the mother liquor and frozen in liquid nitrogen prior to data collection.

Data collection and structure determination

Data were collected from a Se-Met substituted crystal at the beamline X9B at the National Synchrotron Light Source, Brookhaven National Laboratory. Three data sets were collected (0.97915 Å [peak], 0.97946 Å [inflection], and 0.96422 Å [remote]), reduced, and scaled with HKL2000 (Otwinowski and Minor, 1997). Details of data collection are summarized in Table 1.

The structure was solved with the MAD method. A Se-Met substructure was found from peak data with SHELXD (Schneider and Sheldrick, 2002). An initial map was obtained from a single wavelength with SHARP. Due to low solvent content, a better map was obtained with the use of three wavelengths with SHARP (de La Fortelle and Bricogne, 1997) and subsequently SOLVE/RESOLVE (Terwilliger, 2002). We extended the initial model built by RESOLVE by manual building with O (Jones et al., 1991). We followed the refinement with CNS (Brunger et al., 1998) using the simulated annealing protocol (Brunger et al., 1990) with manual rebuilding taking into account the 2-fold noncrystallographic symmetry (NCS). We used a subset of reflections (5%) for R_{free} calculations (Brunger, 1992). Final steps of the refinement were carried out with REFMAC (Murshudov et al., 1997) without NCS restraints. The refinement statistics are summarized in Table 1. Data collected at 0.97915 Å (peak) were used during refinement. The PROCHECK and MOLPROBITY programs were used for structure validation. The final model contains two protein chains and 59 water molecules.

Sedimentation velocity measurements

Samples were equilibrated by dialysis into a buffer containing 50 mM Tris (pH 7.5), 150 mM NaCl, and either 1 mM DTT (NHR2 and m4) or 0.5 mM TCEP (m7) (pH 7.5). Extinction coefficients, molecular masses, and partial specific volumes were determined using the SEDNTERP program (Laue et al., 1992). Sedimentation velocity analytical ultracentrifugation was performed with a Beckman Coulter XL-I instrument in aluminum-filled double sector cells at 20ºC and 50,000 RPM using a scan interval of ~260 s. The sedimentation velocity concentration profiles were fit to finite element solutions of the Lamm equation using a model of a continuous distribution of discrete, noninteracting species with the program SEDFIT (Schuck, 2000). The molecular mass and sedimentation coefficient of the predominant species were determined using a hybrid discrete-continuous model where the major peak was fit as a single discrete species and the material at higher and lower S was accounted for by two continuous distributions. Data obtained at multiple concentrations were globally fit using SEPHAT (Schuck, 2003). Hydrodynamic bead modeling was performed using the crystallographic coordinates for the NHR2 domain using the HYDROPRO package (Garcia De La Torre et al., 2000) with the default effective atomic radii of 3.2 Å.

Western blots

Western blots were performed using standard protocols (details provided in Supplemental Data).

Coimmunoprecipitations

Coimmunoprecipitations were performed using standard protocols (details provided in Supplemental Data).

Retroviral transduction

Phoenix cells were plated in 10 cm dishes in DMEM supplemented with 10% fetal calf serum and penicillin/streptomycin (FCS, P/S), and transfected after 12–16 hr with 20 μg of MigR1 plasmids by calcium phosphate in the presence of chloroquine, and viral supernatants were harvested at 48 hr. Cells were subjected to 2 hr of spinoculation at 2350 RPM, 25ºC in the presence of polybrene, and then cultured for 48 hr with viral supernatant. We determined transduction efficiencies by assessing the percentage of GFP-positive NIH 3T3 cells with a FACScan flow cytometer (BD Bioscience). Expression of AML1/ETO proteins was assessed by Western blots of nuclear extracts prepared from transduced NIH 3T3 cells.

Granulocyte differentiation

Bone marrow (BM) was harvested from male C57BL/6 × 129Sv (F1) mice and cultured for 2 days in DMEM plus FCS P/S, 10 ng/ml IL-3, 20 ng/ml IL-6, 100 ng/ml SCF (R&D Systems). Cells expressing lineage markers were depleted using a cocktail of antibodies conjugated to magnetic beads (Miltenyi). Lineage-negative (Lin^-) cells were infected with retroviruses expressing GFP alone, or GFP in combination with AML1/ETO proteins, and cultured for 7 days in DMEM FCS P/S, 10 ng/ml IL-3, 20 ng/ml IL-6, 100 ng/ml SCF, 60 ng/ml G-CSF (R&D Systems). Cells were harvested and stained for surface expression of Mac1 and Gr-1 (Ly-6C) with antibodies conjugated to PE or APC, respectively (BD Bioscience) using a FACSCalibur flow cytometer (BD Bioscience), and the data were analyzed using FloJo software.

Serial replating

Immediately following retroviral transduction, 10^3 cells were plated in M3434 complete methylcellulose media (Stem Cell Technologies) and cultured for 7 days. After colonies were enumerated, the cultures were diluted and resuspended, and 10^4 cells were replated in M3434 media for an additional 7 days, at which point the process was iteratively repeated as indicated. Cytospins of cells resulting from replatings were generated using a Shandon cytospin and stained with Wright Giemsa.

Real-time PCR

Lin^- BM cells were isolated and transduced with MigR1 expressing GFP, AML1/ETO, or m7 as described above. After 48 hr of culture in IL-3, IL-6, and SCF, cells were isolated using a FACSAria Cell Sorting System (BD Bioscience) based on GFP expression and propidium iodide exclusion. Independent FACS analysis of GFP-positive cells stained with a panel of anti-lineage marker antibodies (Miltenyi, Earhardt, CA) revealed a consistent 95%–98% lineage negativity in all samples (data not shown). Total RNA was extracted from sorted cells with RNeasy spin columns and was Dnasel treated (Qiagen Inc, Valencia, CA). RNA integrity was verified by agarose gel electrophoresis and quantified with Nano-Drop1000 (Nano-Drop, Wilmington, DE). Total RNA was subjected to two rounds of T7-based linear amplification using the RiboAmp RNA Amplification kit (Arcturus Inc, Mountain View, CA). Amplified RNA (aRNA) from each sample was used to generate three independent preparations of double-stranded cDNA (dscDNA) for quantitative analysis of gene expression. An aliquot of this material was subjected to a third round of amplification in the presence of biotinylated dUTP using the Bioarray High Yield RNA Transcript Labeling Kit (ENZO, Farmingdale, NY). Biotinylated RNA was used to interrogate pathway-specific oligonucleotide arrays (Hematopoietic Stem Cell and Hematopoiesis, and Cell Cycle; SuperArray, Frederick, MD) as a primary screen to identify differentially expressed genes. Real-time quantitative PCR of candidate AML1/ETO target genes was then performed in triplicate for each sample using SYBR-Green (Applied Biosystems, Foster City, CA) on Applied Biosystems's 7500 Real-Time PCR System. Linear regression analysis of unknown samples was performed using the relative standard curve method.

Supplemental data

The Supplemental Data include Supplemental experimental procedures, one supplemental figure, and one supplemental table and can be found with this article online at http://www.cancercell.org/cgi/content/full/9/4/249/DC1/.

Acknowledgments

We thank Warren Pear for the MigR1 vector, Scott Hiebert for the cDNAs, and Bruce Hug for his helpful advice. We also thank Harry Higgs for help with the SEC experiments and Jason Moore for statistical support. RO1 CA108056 (J.H.B. and N.A.S.) supported this work. M.D.C. is supported by T32 GM08704, and J.J.G. is supported by T32 AR07576. Flow cytometry was done in The Herbert C. Englert Cell Analysis Laboratory, established by a grant from the Fannie E. Rippel Foundation and supported in part by the Core Grant of the Norris Cotton Cancer Center (CA 23108).

Received: August 10, 2005
Revised: January 30, 2006
Accepted: March 6, 2006
Published: April 10, 2006

References

Amann, J.M., Nip, J., Strom, D.K., Lutterbach, B., Harada, H., Lenny, N., Downing, J.R., Meyers, S., and Hiebert, S.W. (2001). ETO, a target of t(8;21) in acute leukemia, makes distinct contacts with multiple histone deacetylases and binds mSin3A through its oligomerization domain. Mol. Cell Biol. *21*, 6470–6483.

Amann, J.M., Chyla, B.J., Ellis, T.C., Martinez, A., Moore, A.C., Franklin, J.L., McGhee, L., Meyers, S., Ohm, J.E., Luce, K.S., et al. (2005). Mtgr1 is a transcriptional corepressor that is required for maintenance of the secretory cell lineage in the small intestine. Mol. Cell Biol. *25*, 9576–9585.

Antonin, W., Fasshauer, D., Becker, S., Jahn, R., and Schneider, T.R. (2002). Crystal structure of the endosomal SNARE complex reveals common structural principles of all SNAREs. Nat. Struct. Biol. *9*, 107–111.

Brunger, A.T. (1992). Free R value: a novel statistical quantity for assessing the accuracy of crystal structures. Nature *335*, 472–475.

Brunger, A.T., Krukowski, A., and Erickson, J.W. (1990). Slow-cooling protocols for crystallographic refinement by simulated annealing. Acta Crystallogr. A *46* (*Pt7*), 585–593.

Brunger, A.T., Adams, P.D., Clore, G.M., DeLano, W.L., Gros, P., Grosse-Kunstleve, R.W., Jiang, J.S., Kuszewski, J., Nilges, M., and Pannu, N.S. (1998). Crystallography & NMR system: A new software suite for macromolecular structure determination. Acta Crystallogr. D Biol. Crystallogr. *54* (*Pt5*), 905–921.

Calabi, F., Pannell, R., and Pavloska, G. (2001). Gene targeting reveals a crucial role for MTG8 in the gut. Mol. Cell Biol. *21*, 5658–5666.

Davis, J.N., McGhee, L., and Meyers, S. (2003). The ETO (MTG8) gene family. Gene *303*, 1–10.

de La Fortelle, E., and Bricogne, G. (1997). Maximum-likelihood heavy-atom parameter refinement for multiple isomorphous replacement and multiwavelength anomalous diffraction methods. Methods Enzymol. *276*, 472–494.

Eguchi, M., Eguchi-Ishimae, M., and Greaves, M. (2004). The small oligomerization domain of gephyrin converts MLL to an oncogene. Blood *103*, 3876–3882.

Elagib, K.E., Racke, F.K., Mogass, M., Khetawat, R., Delehanty, L.L., and Goldfarb, A.N. (2003). RUNX1 and GATA-1 coexpression and cooperation in megakaryocytic differentiation. Blood *101*, 4333–4341.

Fasshauer, D., Sutton, R.B., Brunger, A.T., and Jahn, R. (1998). Conserved structural features of the synaptic fusion complex: SNARE proteins reclassified as Q- and R-SNAREs. Proc. Natl. Acad. Sci. USA *95*, 15781–15786.

Fukuyama, T., Sueoka, E., Sugio, Y., Otsuka, T., Niho, Y., Akagi, K., and Kozu, T. (2001). MTG8 proto-oncoprotein interacts with the regulatory subunit of type II cyclic AMP-dependent protein kinase in lymphocytes. Oncogene *20*, 6225–6232.

Gamou, T., Kitamura, E., Hosoda, F., Shimizu, K., Shinohara, K., Hayashi, Y., Nagase, T., Yokoyama, Y., and Ohki, M. (1998). The partner gene of AML1 in t(16;21) myeloid malignancies is a novel member of the MTG8(ETO) family. Blood *91*, 4028–4037.

Garcia De La Torre, J., Huertas, M.L., and Carrasco, B. (2000). Calculation of hydrodynamic properties of globular proteins from their atomic-level structure. Biophys. J. *78*, 719–730.

Gelmetti, V., Zhang, J., Fanelli, M., Minucci, S., Pelicci, P.G., and Lazar, M.A. (1998). Aberrant recruitment of the nuclear receptor corepressor-histone deacetylase complex by the acute myeloid leukemia fusion partner ETO. Mol. Cell Biol. *18*, 7185–7191.

Growney, J.D., Shigematsu, H., Li, Z., Lee, B.H., Adelsperger, J., Rowan, R., Curley, D.P., Kutok, J.L., Akashi, K., Williams, I.R., et al. (2005). Loss of Runx1 perturbs adult hematopoiesis and is associated with a myeloproliferative phenotype. Blood *106*, 494–504.

Harbury, P.B., Zhang, T., Kim, P.S., and Alber, T. (1993). A switch between two-, three-, and four-stranded coiled coils in GCN4 leucine zipper mutants. Science *262*, 1401–1407.

Hiebert, S.W., Lutterbach, B., and Amann, J. (2001). Role of co-repressors in transcriptional repression mediated by the t(8;21), t(16;21), t(12;21), and inv(16) fusion proteins. Curr. Opin. Hematol. *8*, 197–200.

Higuchi, M., O'Brien, D., Kumaravelu, P., Lenny, N., Yeoh, E.J., and Downing, J.R. (2002). Expression of a conditional AML1-ETO oncogene bypasses embryonic lethality and establishes a murine model of human t(8;21) acute myeloid leukemia. Cancer Cell *1*, 63–74.

Hildebrand, D., Tiefenbach, J., Heinzel, T., Grez, M., and Maurer, A.B. (2001). Multiple regions of ETO cooperate in transcriptional repression. J. Biol. Chem. *276*, 9889–9895.

Hug, B.A., and Lazar, M.A. (2004). ETO interacting proteins. Oncogene *23*, 4270–4274.

Hug, B.A., Lee, S.Y., Kinsler, E.L., Zhang, J., and Lazar, M.A. (2002). Cooperative function of Aml1-ETO corepressor recruitment domains in the expansion of primary bone marrow cells. Cancer Res. *62*, 2906–2912.

Ichikawa, M., Asai, T., Saito, T., Yamamoto, G., Seo, S., Yamazaki, I., Yamagata, T., Mitani, K., Chiba, S., Ogawa, S., et al. (2004). AML-1 is required for megakaryocytic maturation and lymphocytic differentiation, but not for maintenance of hematopoietic stem cells in adult hematopoiesis. Nat. Med. *10*, 299–304.

Jones, T.A., Zou, J.Y., Cowan, S.W., and Kjeldgaard. (1991). Improved methods for building protein models in electron density maps and the location of errors in these models. Acta Crystallogr. A *47*, 110–119.

Kitabayashi, I., Ida, K., Morohoshi, F., Yokoyama, A., Mitsuhashi, N., Shimizu, K., Nomura, N., Hayashi, Y., and Ohki, M. (1998). The AML1-MTG8 leukemic fusion protein forms a complex with a novel member of the MTG8(ETO/CDR) family, MTGR1. Mol. Cell Biol. *18*, 846–858.

Kumar, S., and Nussinov, R. (1999). Salt bridge stability in monomeric proteins. J. Mol. Biol. *293*, 1241–1255.

Laue, T.M., Shah, B.D., Ridgeway, T.M., and Pelletier, S.L. (1992). Computer-Aided Interpretation of Analytical Sedimentation Data for Proteins (Cambridge: Royal Society of Chemistry).

Lin, R.J., and Evans, R.M. (2000). Acquisition of oncogenic potential by RAR chimeras in acute promyelocytic leukemia through formation of homodimers. Mol. Cell *5*, 821–830.

Lutterbach, B., Sun, D., Schuetz, J., and Hiebert, S.W. (1998a). The MYND motif is required for repression of basal transcription from the multidrug resistance 1 promoter by the t(8;21) fusion protein. Mol. Cell Biol. *18*, 3604–3611.

Lutterbach, B., Westendorf, J.J., Linggi, B., Patten, A., Moniwa, M., Davie, J.R., Huynh, K.D., Bardwell, V.J., Lavinsky, R.M., Rosenfeld, M.G., et al. (1998b). ETO, a target of t(8;21) in acute leukemia, interacts with the N-CoR and mSin3 corepressors. Mol. Cell Biol. *18*, 7176–7184.

Martin, M.E., Milne, T.A., Bloyer, S., Galoian, K., Shen, W., Gibbs, D., Brock, H.W., Slany, R., and Hess, J.L. (2003). Dimerization of MLL fusion proteins immortalizes hematopoietic cells. Cancer Cell *4*, 197–207.

McGhee, L., Bryan, J., Elliott, L., Grimes, H.L., Kazanjian, A., Davis, J.N., and Meyers, S. (2003). Gfi-1 attaches to the nuclear matrix, associates with ETO (MTG8) and histone deacetylase proteins, and represses transcription using a TSA-sensitive mechanism. J. Cell Biochem. *89*, 1005–1018.

McKercher, S.R., Torbett, B.E., Anderson, K.L., Henkel, G.W., Vestal, D.J., Baribault, H., Klemsz, M., Feeney, A.J., Wu, G.E., Paige, C.J., and Maki, R.A. (1996). Targeted disruption of the PU.1 gene results in multiple hematopoietic abnormalities. EMBO J. *15*, 5647–5658.

McWhirter, J.R., Galasso, D.L., and Wang, J.Y. (1993). A coiled-coil oligomerization domain of Bcr is essential for the transforming function of Bcr-Abl oncoproteins. Mol. Cell Biol. *13*, 7587–7595.

Melnick, A., and Licht, J.D. (1999). Deconstructing a disease: RARα, its fusion partners, and their roles in the pathogenesis of acute promyelocytic leukemia. Blood *93*, 3167–3215.

Minucci, S., Maccarana, M., Cioce, M., De Luca, P., Gelmetti, V., Segalla, S., Di Croce, L., Giavara, S., Matteucci, C., Gobbi, A., et al. (2000). Oligomerization of RAR and AML1 transcription factors as a novel mechanism of oncogenic activation. Mol. Cell *5*, 811–820.

Miyoshi, H., Kozu, T., Shimizu, K., Enomoto, K., Maseki, N., Kaneko, Y., Kamada, N., and Ohki, M. (1993). The t(8;21) translocation in acute myeloid leukemia results in production of an AML1-MTG8 fusion transcript. EMBO J. *12*, 2715–2721.

Mulloy, J.C., Cammenga, J., MacKenzie, K.L., Berguido, F.J., Moore, M.A., and Nimer, S.D. (2002). The AML1-ETO fusion protein promotes the expansion of human hematopoietic stem cells. Blood *99*, 15–23.

Murshudov, G.N., Vagin, A.A., and Dodson, E.J. (1997). Free R value: a novel statistical quantity for assessing the accuracy of crystal structures. Acta Crystallogr. D Biol. Crystallogr. *53*, 240–255.

Okuda, T., van Deursen, J., Hiebert, S.W., Grosveld, G., and Downing, J.R. (1996). AML1, the target of multiple chromosomal translocations in human leukemia, is essential for normal fetal liver hematopoiesis. Cell *84*, 321–330.

Otto, F., Lubbert, M., and Stock, M. (2003). Upstream and downstream targets of RUNX proteins. J. Cell Biochem. *89*, 9–18.

Otwinowski, Z., and Minor, W. (1997). Processing of X-ray diffraction data collected in oscillation mode. Methods Enzymol. *276*, 307–326.

Peterson, L.F., and Zhang, D.E. (2004). The 8;21 translocation in leukemogenesis. Oncogene *23*, 4255–4262.

Ponstingl, H., Henrick, K., and Thornton, J.M. (2000). Discriminating between homodimeric and monomeric proteins in the crystalline state. Proteins *41*, 47–57.

Rosenbauer, F., Wagner, K., Kutok, J.L., Iwasaki, H., Le Beau, M.M., Okuno, Y., Akashi, K., Fiering, S., and Tenen, D.G. (2004). Acute myeloid leukemia induced by graded reduction of a lineage-specific transcription factor, PU.1. Nat. Genet. *36*, 624–630.

Rosenbauer, F., Owens, B.M., Yu, L., Tumang, J.R., Steidl, U., Kutok, J.L., Clayton, L.K., Wagner, K., Scheller, M., Iwasaki, H., et al. (2006). Lymphoid cell growth and transformation are suppressed by a key regulatory element of the gene encoding PU.1. Nat. Genet. *38*, 27–37.

Schneider, T.R., and Sheldrick, G.M. (2002). Substructure solution with SHELXD. Acta Crystallogr. D Biol. Crystallogr. *58*, 1772–1779.

Schuck, P. (2000). Size-distribution analysis of macromolecules by sedimentation velocity ultracentrifugation and lamm equation modeling. Biophys. J. *78*, 1606–1619.

Schuck, P. (2003). On the analysis of protein self-association by sedimentation velocity analytical ultracentrifugation. Anal. Biochem. *320*, 104–124.

Schuh, A.H., Tipping, A.J., Clark, A.J., Hamlett, I., Guyot, B., Iborra, F.J., Rodriguez, P., Strouboulis, J., Enver, T., Vyas, P., and Porcher, C. (2005). ETO-2 associates with SCL in erythroid cells and megakaryocytes and provides repressor functions in erythropoiesis. Mol. Cell Biol. *25*, 10235–10250.

Scott, E.W., Simon, M.C., Anastasi, J., and Singh, H. (1994). Requirement of transcription factor PU.1 in the development of multiple hematopoietic lineages. Science *265*, 1573–1577.

Shimada, H., Ichikawa, H., Nakamura, S., Katsu, R., Iwasa, M., Kitabayashi, I., and Ohki, M. (2000). Analysis of genes under the downstream control of the t(8;21) fusion protein AML1-MTG8: overexpression of the TIS11b (ERF-1, cMG1) gene induces myeloid cell proliferation in response to G-CSF. Blood *96*, 655–663.

Shimada, H., Ichikawa, H., and Ohki, M. (2002). Potential involvement of the AML1-MTG8 fusion protein in the granulocytic maturation characteristic of the t(8;21) acute myelogenous leukemia revealed by microarray analysis. Leukemia *16*, 874–885.

So, C.W., and Cleary, M.L. (2004). Dimerization: a versatile switch for oncogenesis. Blood *104*, 919–922.

Spek, E.J., Bui, A.H., Lu, M., and Kallenbach, N.R. (1998). Surface salt bridges stabilize the GCN4 leucine zipper. Protein Sci. *7*, 2431–2437.

Sutton, R.B., Fasshauer, D., Jahn, R., and Brunger, A.T. (1998). Crystal structure of a SNARE complex involved in synaptic exocytosis at 2.4 A resolution. Nature *395*, 347–353.

Terwilliger, T.C. (2002). Automated structure solution, density modification and model building. Acta Crystallogr. D Biol. Crystallogr. *58*, 1937–1940.

Vangala, R.K., Heiss-Neumann, M.S., Rangatia, J.S., Singh, S.M., Schoch, C., Tenen, D.G., Hiddemann, W., and Behre, G. (2003). The myeloid master regulator transcription factor PU.1 is inactivated by AML1-ETO in t(8;21) myeloid leukemia. Blood *101*, 270–277.

Wang, Q., Stacy, T., Binder, M., Marin-Padilla, M., Sharpe, A.H., and Speck, N.A. (1996). Disruption of the Cbfa2 gene causes necrosis and hemorrhaging in the central nervous system and blocks definitive hematopoiesis. Proc. Natl. Acad. Sci. USA *93*, 3444–3449.

Wang, J., Hoshino, T., Redner, R.L., Kajigaya, S., and Liu, J.M. (1998). ETO, fusion partner in t(8;21) acute myeloid leukemia, represses transcription by interaction with the human N-CoR/mSin3/HDAC1 complex. Proc. Natl. Acad. Sci. USA *95*, 10860–10865.

Wildonger, J., and Mann, R.S. (2005). Evidence that nervy, the Drosophila homolog of ETO/MTG8, promotes mechanosensory organ development by enhancing Notch signaling. Dev. Biol. *286*, 507–520.

Yan, M., Burel, S.A., Peterson, L.F., Kanbe, E., Iwasaki, H., Boyapati, A., Hines, R., Akashi, K., and Zhang, D.E. (2004). Deletion of an AML1-ETO C-terminal NcoR/SMRT-interacting region strongly induces leukemia development. Proc. Natl. Acad. Sci. USA *101*, 17186–17191.

Yang, H.T., Wu, D.H., Xue, X.Y., Liang, W.X., Miao, X.Y., Pang, H., and Chen, S.J. (2004). Cloning, expression, purification and crystallization of NHR3 domain from acute myelogenous leukemia-related protein AML1-ETO. Acta Biochim. Biophys. Sin. (Shanghai) *36*, 566–570.

Zhang, J., Hug, B.A., Huang, E.Y., Chen, C.W., Gelmetti, V., Maccarana, M., Minucci, S., Pelicci, P.G., and Lazar, M.A. (2001). Oligomerization of ETO is obligatory for corepressor interaction. Mol. Cell Biol. *21*, 156–163.

Zhang, J., Kalkum, M., Yamamura, S., Chait, B.T., and Roeder, R.G. (2004). E protein silencing by the leukemogenic AML1-ETO fusion protein. Science *305*, 1286–1289.

Accession numbers

The coordinates and structure factors are deposited in the Protein Data Bank with accession code 1WQ6.